Electronic Supplementary Information (ESI) for New Journal of Chemistry

Construction of highly dispersed Au active sites by ice photochemical polishing for efficient acetylene hydrochlorination

Lisha Yao,[a] Haiyang Zhang,*[a] Yanqin Li,[a] Miaomiao Zhang,[a] Feng Li,[a] Linfeng Li, [a] and Jinli Zhang *[a,b]

[a] School of Chemistry and Chemical Engineering/Key Laboratory for Green Processing of Chemical Engineering of Xinjiang Bingtuan, Shihezi University, Shihezi 832000 (P.R. China); E-mail: zhy198722@163.com (H.Y. Zhang).

[b] School of Chemical Engineering and Technology, Tianjin University, Tianjin 300072 (P.R. China); E-mail: zhangjinli@tju.edu.cn (J.L. Zhang).

*Corresponding authors: Tel: +86-993-2057-277;

E-mail: zhy198722@163.com (H.Y. Zhang), and zhangjinli@tju.edu.cn (J.L. Zhang).

Captions of Figures and Tables

Fig. S1 Schematic of the microreactor for acetylene hydrochlorination.

Fig. S2 Acetylene conversion rate (a) and selectivity to VCM (b) over the prepared Au-based catalysts. Reaction conditions: temperature = 180 °C, GHSV (C_2H_2) = 1200 h^{-1}, and V_{HCl}/V_{C2H2} = 1.15.

Fig. S3 Acetylene conversion rate (a) and selectivity to VCM (b) over the prepared Au/AC-F_xI_y catalysts. Reaction conditions: temperature = 180 °C, GHSV (C_2H_2) = 1200 h^{-1}, and V_{HCl}/V_{C2H2} = 1.15.

Fig. S4 Nitrogen adsorption and desorption isotherms of unreacted (a) and reacted (b) Au/AC-F_xI_y catalysts.

Fig. S5 TG/DTG curves of the unreacted and reacted Au/AC-F_xI_y catalysts.

Fig. S6 XRPD patterns of the unreacted (a) and reacted (b) Au/AC-F_xI_y catalysts.

Fig. S7 TEM images of the unreacted (left) and reacted (right) catalysts: AC (a, b), Au/AC-F_1I_0 (c, d), Au/AC-$F_{0.5}I_{0.5}$ (e, f), Au/AC-$F_{1.5}I_{1.5}$ (g, h), Au/AC-F_2I_2 (i, j), and Au/AC-F_0I_1 (k, l); about 150 particles were measured for the unreacted and reacted samples.

Fig. S8 HAADF-STEM images of the unreacted catalysts: Au/AC-F_1I_1 (a) and Au/AC-$F_{1.5}I_{1.5}$ (b).

Fig. S9 The constraint relationships between catalytic activity and Au nanoparticle size.

Fig. S10 TPR profiles of the unreacted Au/AC-F_xI_y catalysts.

Fig. S11 Au 4*f* XPS spectra and valence distribution of the unreacted (a) and reacted (b) catalysts.

Fig. S12 Changes in the Au^{n+} content of unreacted Au/AC-F_xI_y catalysts after different times of UV light irradiation.

Fig. S13 Wavelet transform plots analysis of Au foil (a), AuCl (b), $AuCl_3$ (c), Au/AC (d), and Au/AC-F_1I_1 (e).

Fig. S14 UV–vis adsorption spectra of the Au solution.

Fig. S15 C_2H_2-TPD (a) and HCl-TPD (b) profiles of the unreacted Au/AC-F_xI_y catalysts.

Table S1 The physical properties of different Au-based catalysts.

Table S2 The amount of coke deposition on the catalysts.

Table S3 The average particle size determined from XRPD patterns by Scherrer equation.

Table S4 EXAFS fitting parameters at the Au L_3-edge for various samples（S_0^2=0.81）

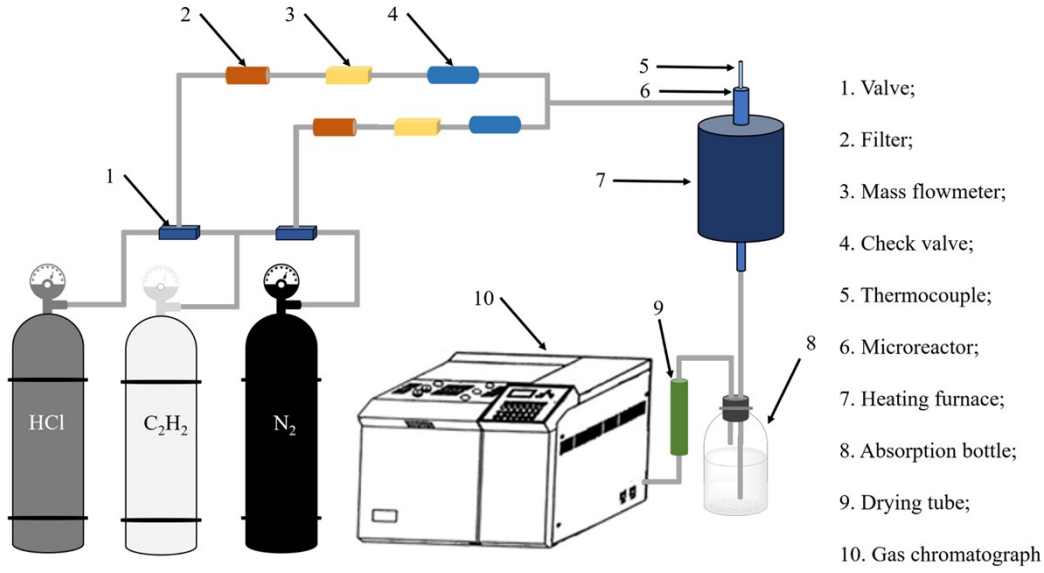

Fig. S1 Schematic of the microreactor for acetylene hydrochlorination.

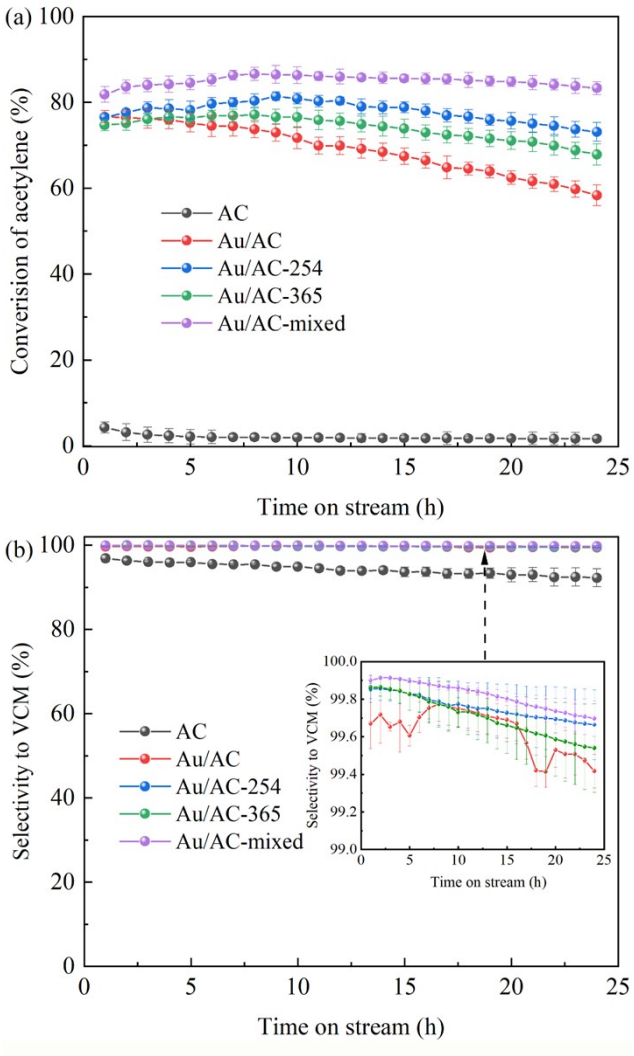

Fig. S2 Acetylene conversion rate (a) and selectivity to VCM (b) over the prepared Au-based catalysts. Reaction conditions: temperature = 180 °C, GHSV (C_2H_2) = 1200 h^{-1}, and V_{HCl}/V_{C2H2} = 1.15.

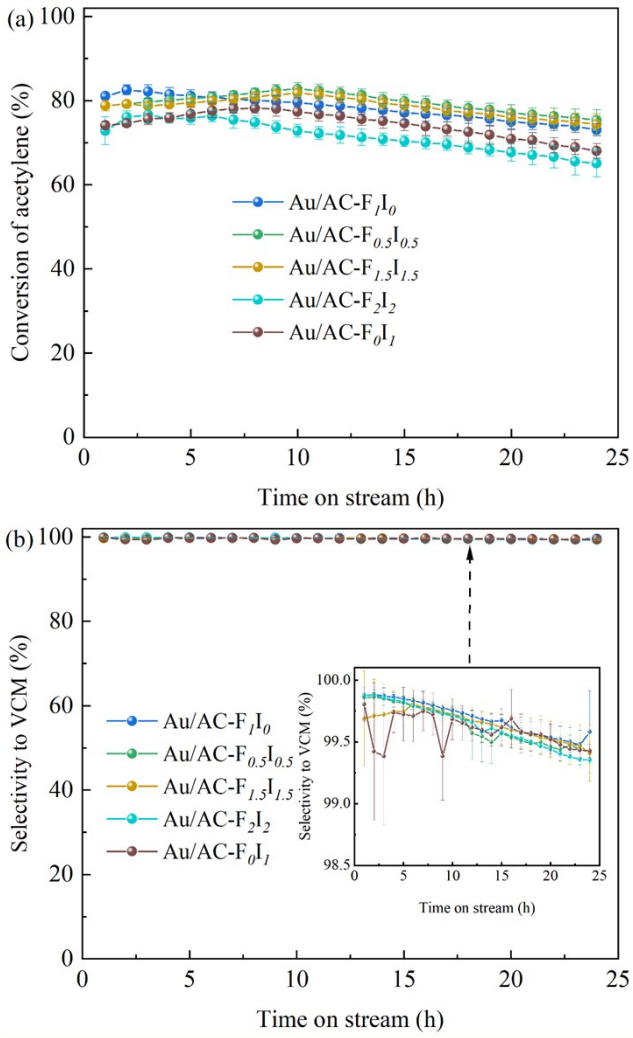

Fig. S3 Acetylene conversion rate (a) and selectivity to VCM (b) over the prepared Au/AC-F_xI_y catalysts. Reaction conditions: temperature = 180 °C, GHSV (C_2H_2) = 1200 h^{-1}, and V_{HCl}/V_{C2H2} = 1.15.

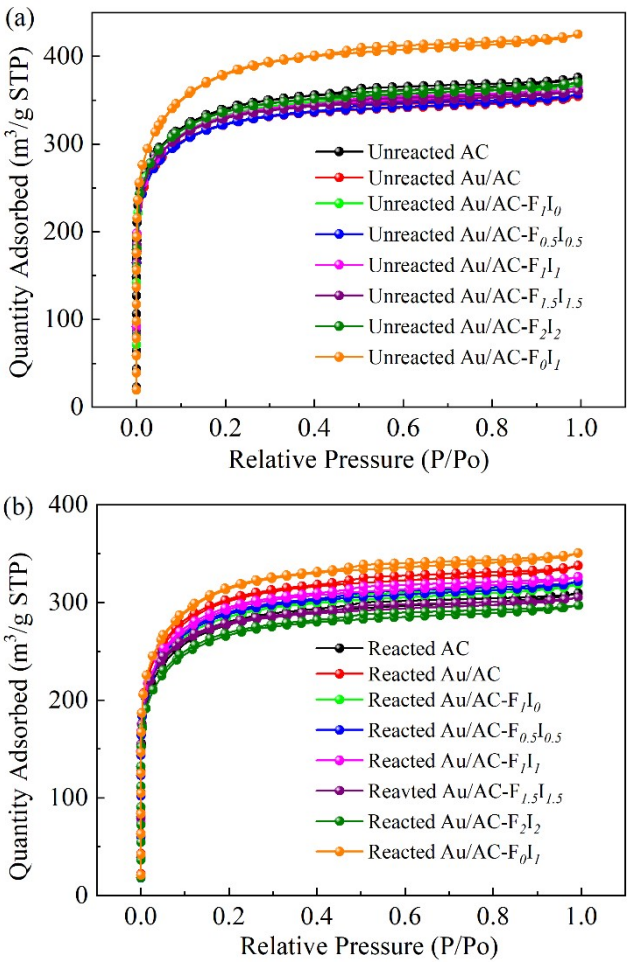

Fig. S4 Nitrogen adsorption and desorption isotherms of unreacted (a) and reacted (b) Au/AC-F_xI_y catalysts.

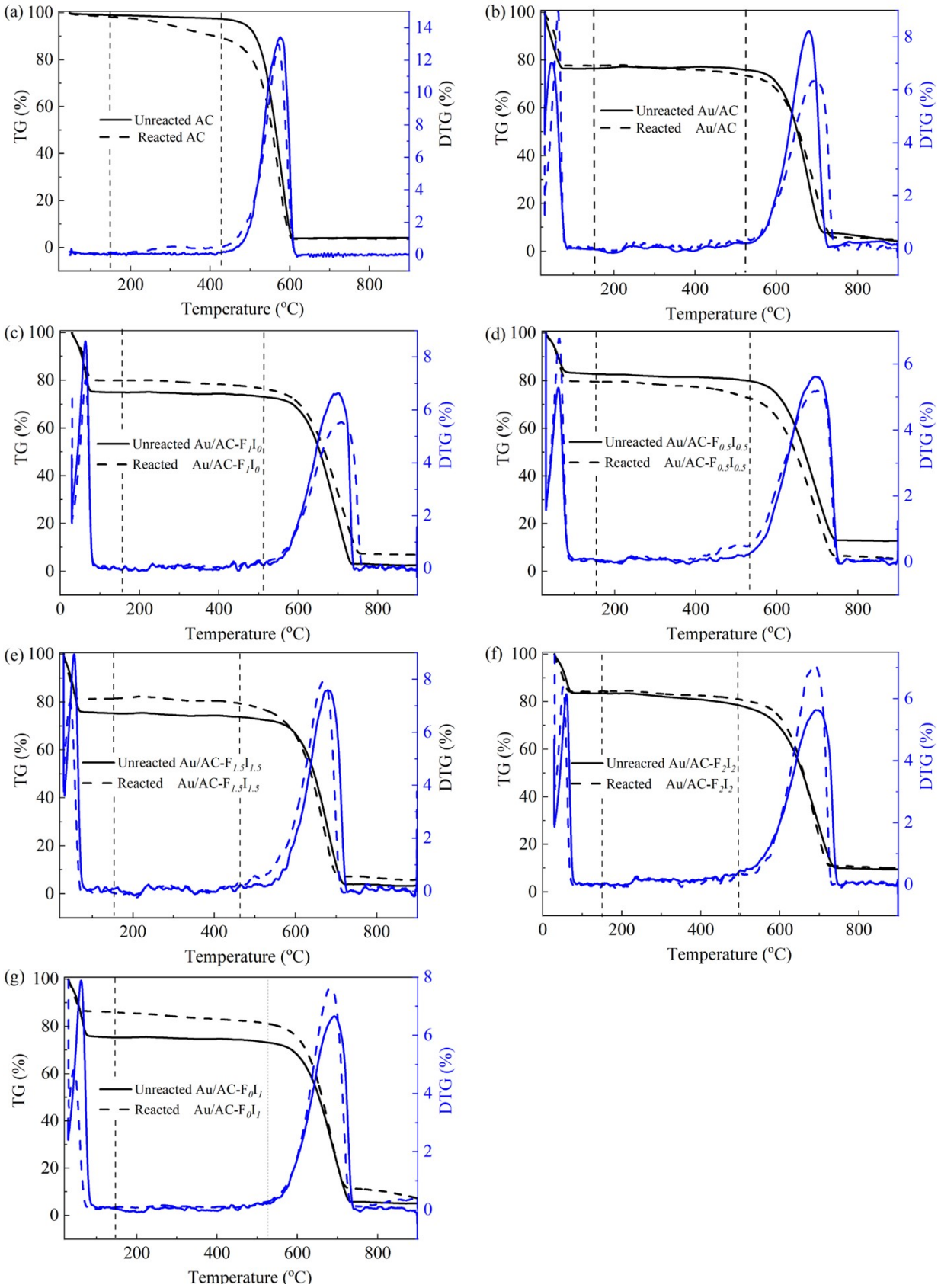

Fig. S5 TG/DTG curves of the unreacted and reacted Au/AC-F_xI_y catalysts.

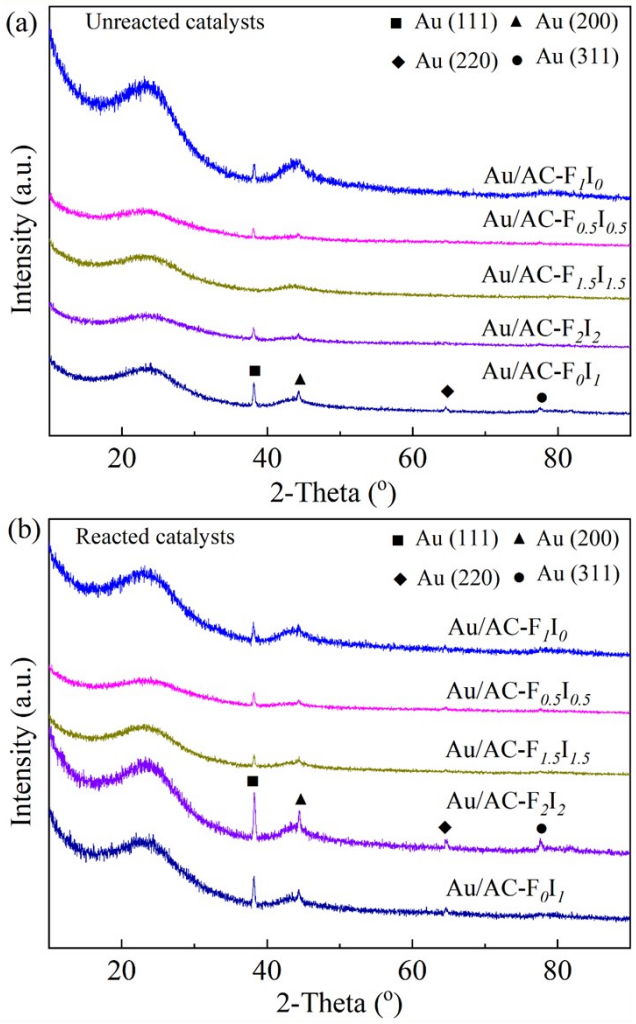

Fig. S6 XRPD patterns of the unreacted (a) and reacted (b) Au/AC-F_xI_y catalysts.

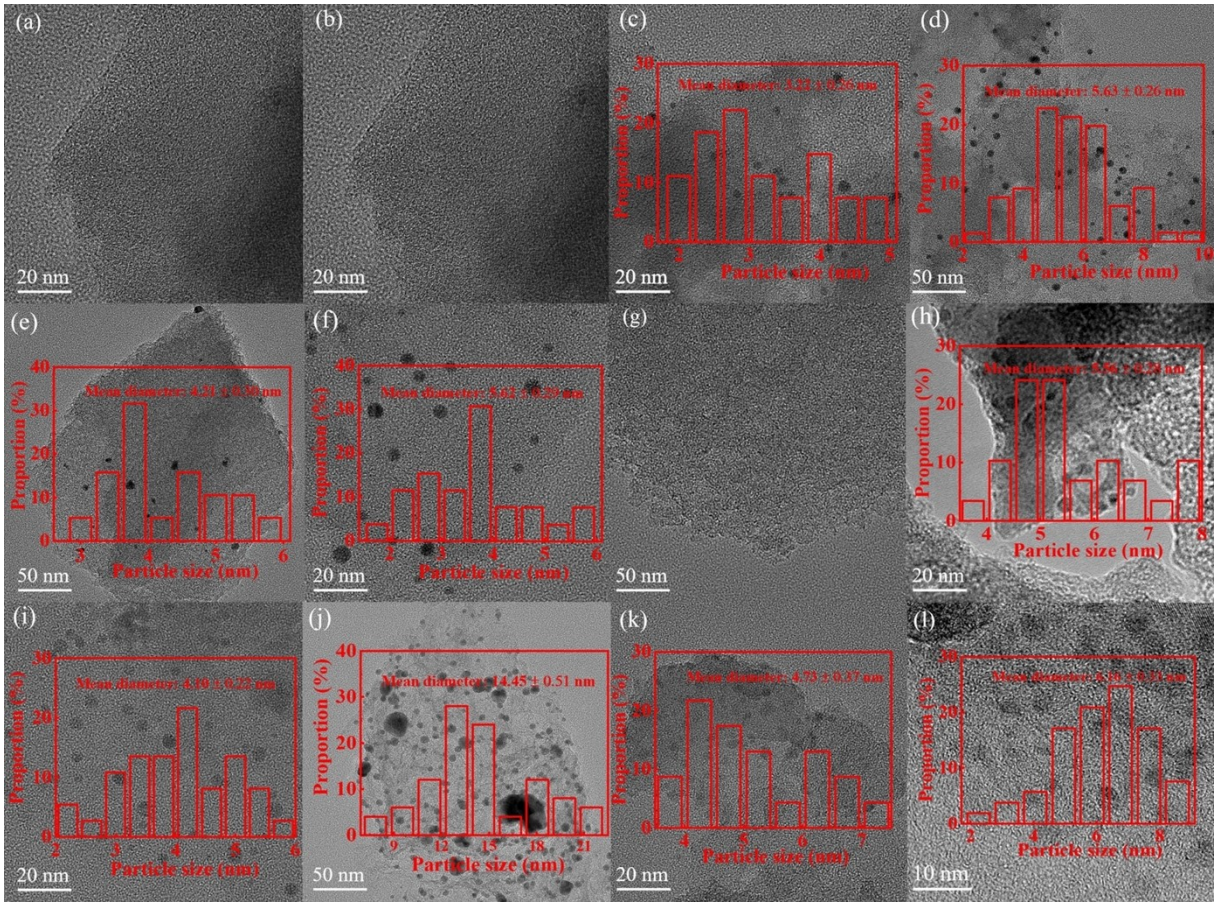

Fig. S7 TEM images of the unreacted (left) and reacted (right) catalysts: AC (a, b), Au/AC-F_1I_0 (c, d), Au/AC-$F_{0.5}I_{0.5}$ (e, f), Au/AC-$F_{1.5}I_{1.5}$ (g, h), Au/AC-F_2I_2 (i, j), and Au/AC-F_0I_1 (k, l); about 150 particles were measured for the unreacted and reacted samples.

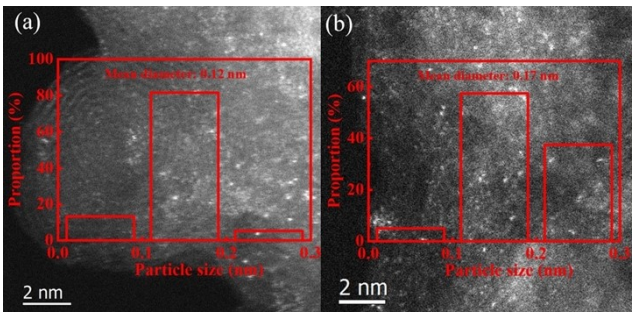

Fig. S8 HAADF-STEM images of the unreacted catalysts: Au/AC-F_1I_1 (a) and Au/AC-$F_{1.5}I_{1.5}$ (b).

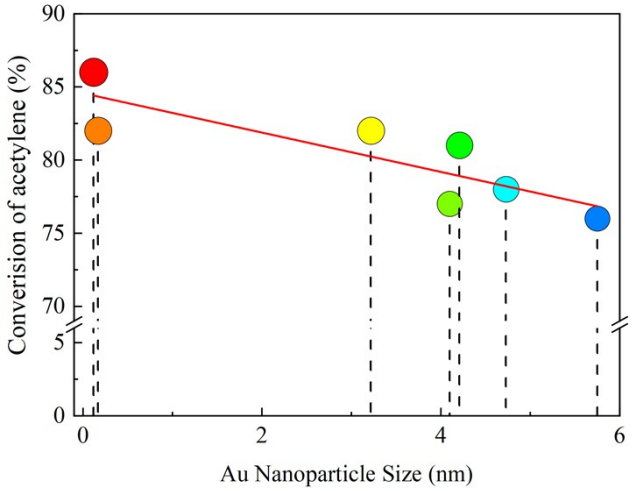

Fig. S9 The constraint relationships between catalytic activity and Au nanoparticle size.

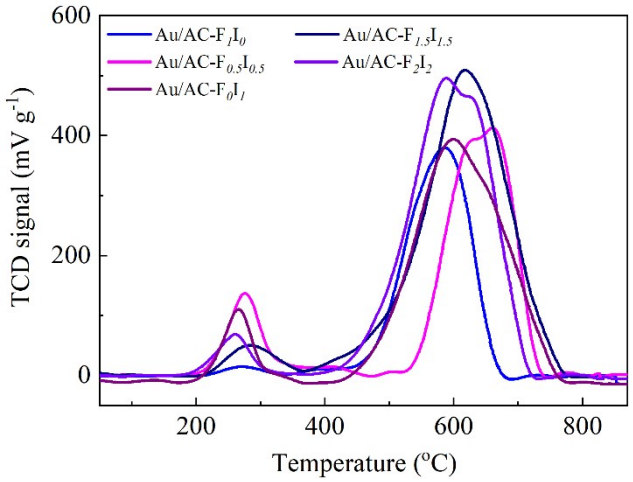

Fig. S10 TPR profiles of the unreacted Au/AC-F_xI_y catalysts.

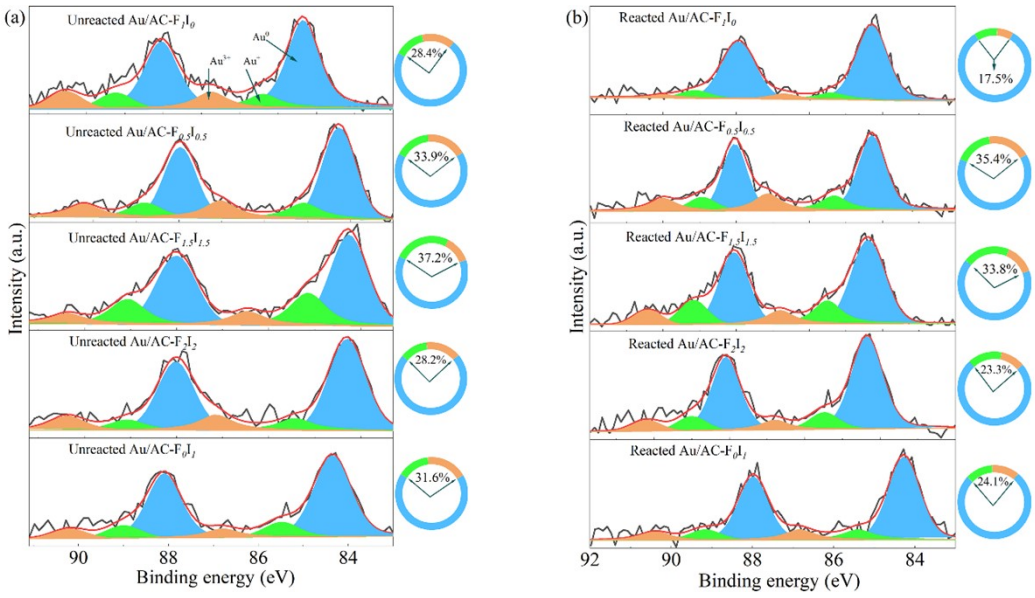

Fig. S11 Au 4*f* XPS spectra and valence distribution of the unreacted (a) and reacted (b) catalysts.

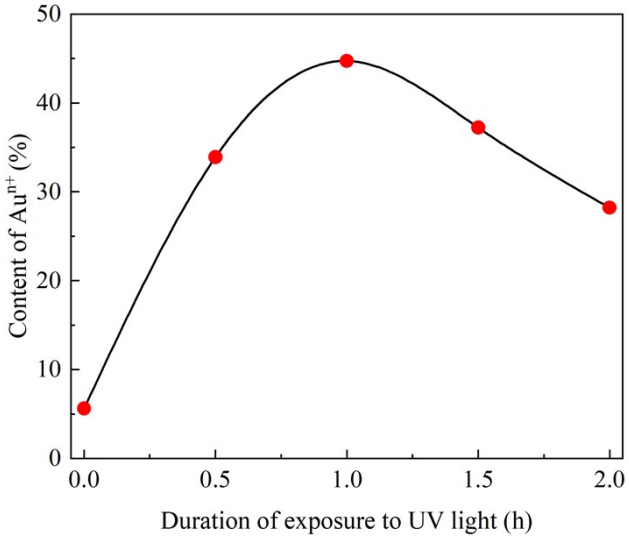

Fig. S12 Changes in the Au^{n+} content of unreacted Au/AC-F_xI_y catalysts after different times of UV light irradiation.

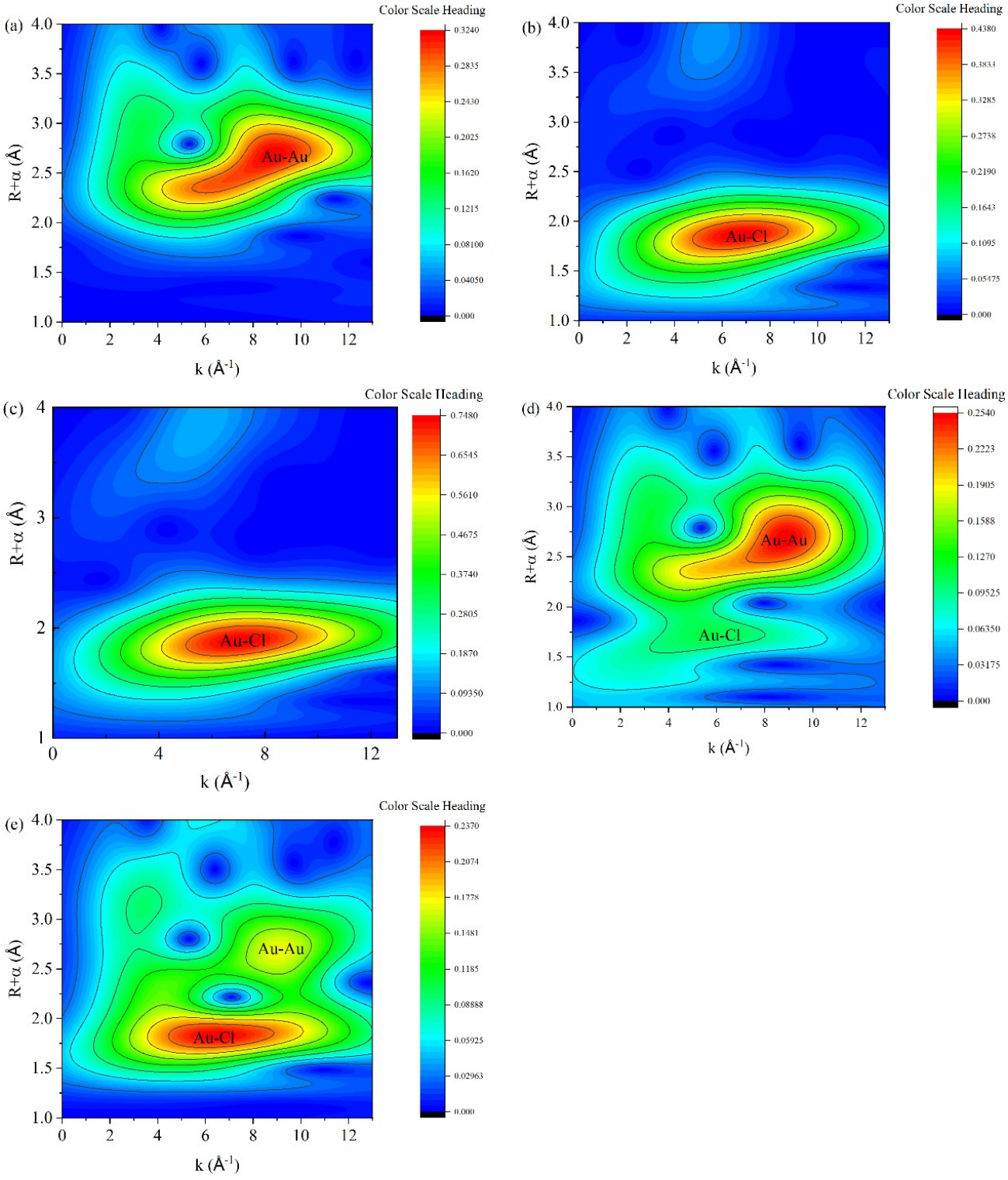

Fig. S13 Wavelet transform plots analysis of Au foil (a), AuCl (b), $AuCl_3$ (c), Au/AC (d), and Au/AC-F_1I_1 (e).

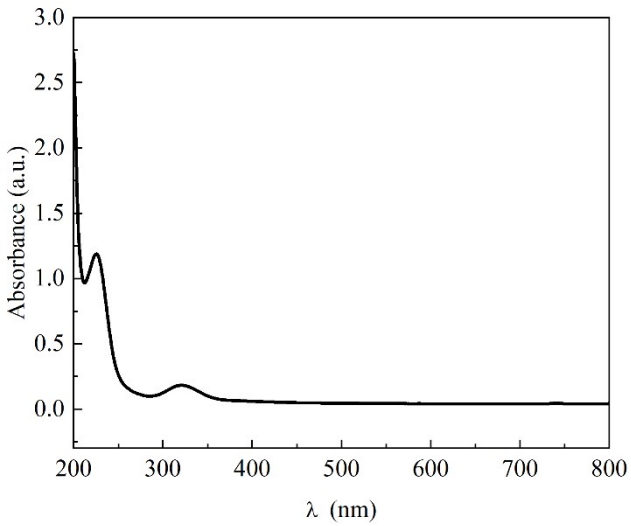

Fig. S14 UV–vis adsorption spectra of the Au solution.

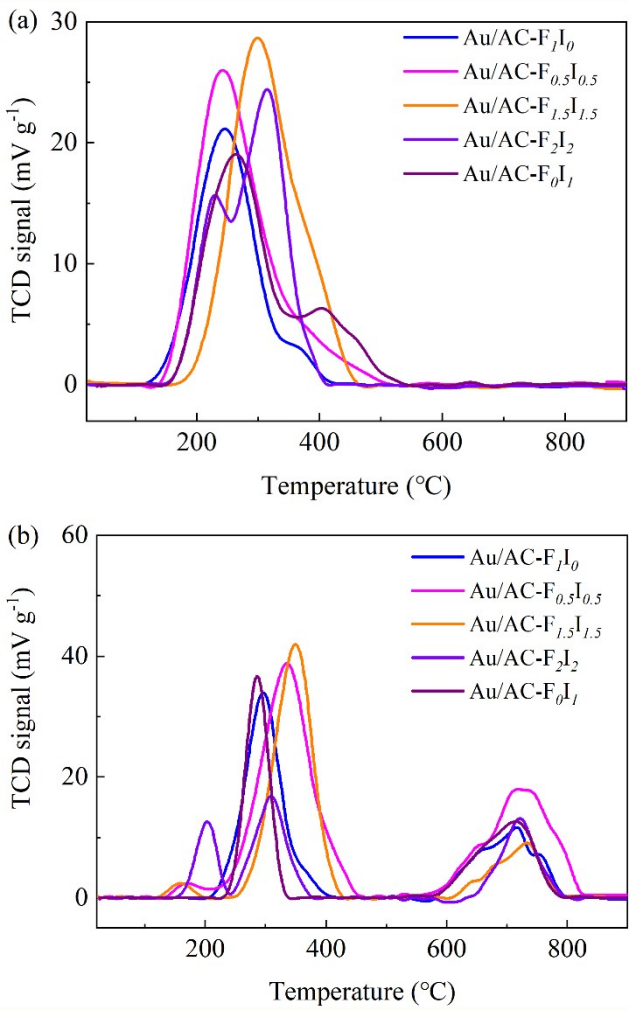

Fig. S15 C_2H_2-TPD (a) and HCl-TPD (b) profiles of the unreacted Au/AC-F_xI_y catalysts.

Table S1 The physical properties of the different Au-based catalysts.

Samples	S_{BET}[a] ($m^2\ g^{-1}$)	$\triangle S_{BET}$ (%)	$S_{micro.}$[b] ($m^2\ g^{-1}$)	S_{micro}/S_{BET} (%)	$S_{ext.}$[c] ($m^2\ g^{-1}$)	S_{ext}/S_{BET} (%)	V_P[d] ($cm^3\ g^{-1}$)	$\triangle V_P$ (%)	$V_{micro.}$[e] ($cm^3\ g^{-1}$)	$V_{ext.}$ ($cm^3\ g^{-1}$)	D_{pore}[f] (nm)
Unreacted AC	1143	31.8	719	62.9	424	37.11	0.59	35.6	0.35	0.24	2.19
Reacted AC	779		447	57.4	332	42.6	0.38		0.27	0.11	2.21
Unreacted Au/AC	987	25.9	620	62.8	367	37.2	0.55	23.6	0.33	0.22	2.22
Reacted Au/AC	731		436	59.6	295	40.4	0.42		0.23	0.19	2.24
Unreacted Au/AC-F_1I_0	1020	13.7	624	61.2	396	38.8	0.54	13.0	0.33	0.21	2.21
Reacted Au/AC-F_1I_0	880		518	58.9	362	41.1	0.47		0.28	0.19	2.24
Unreacted Au/AC-$F_{0.5}I_{0.5}$	989	10.0	613	62.0	376	38.0	0.56	10.7	0.34	0.22	2.21
Reacted Au/AC-$F_{0.5}I_{0.5}$	890		517	58.1	373	41.9	0.50		0.28	0.22	2.23
Unreacted Au/AC-F_1I_1	1013	4.1	639	63.1	374	36.9	0.56	5.4	0.34	0.22	2.21
Reacted Au/AC-F_1I_1	971		611	62.9	360	37.1	0.53		0.32	0.21	2.23
Unreacted Au/AC-$F_{1.5}I_{1.5}$	1008	7.6	639	63.4	369	36.6	0.55	7.3	0.34	0.21	2.21
Reacted Au/AC-$F_{1.5}I_{1.5}$	931		573	61.5	358	38.5	0.51		0.29	0.22	2.22
Unreacted Au/AC-F_2I_2	1033	20.3	646	62.5	387	37.5	0.57	19.3	0.34	0.23	2.22
Reacted Au/AC-F_2I_2	823		472	57.4	351	42.6	0.46		0.25	0.21	2.23
Unreacted Au/AC-F_0I_1	1043	17.1	669	64.1	374	35.9	0.55	14.5	0.32	0.23	2.21
Reacted Au/AC-F_0I_1	865		531	61.4	334	38.6	0.47		0.29	0.18	2.22

[a] S_{BET}: BET specific surface area; [b] t-plot micropore area; [c] t-plot external surface area; [d] V_P: total pore volume, volume at $p/p_0 = 0.98$;

[e] t-plot micropore volume; [f] Adsorption average pore width (4V/A) by BET.

Table S2 The amount of coke deposition on the catalysts.

Samples	Amount of coke deposition (%)
AC	8.1
Au/AC	4.2
Au/AC-F_1I_0	2.6
Au/AC-$F_{0.5}I_{0.5}$	1.3
Au/AC-F_1I_1	0.6
Au/AC-$F_{1.5}I_{1.5}$	1.2
Au/AC-F_2I_2	2.0
Au/AC-F_0I_1	2.5

Table S3 The average particle size determined from XRPD patterns by Scherrer equation.

Catalysts	Particle size (nm)	
	Fresh	Spent
Au/AC	7.6	16.4
Au/AC-F_1I_0	4.8	7.6
Au/AC-$F_{0.5}I_{0.5}$	4.6	6.7
Au/AC-F_1I_1	< 4.0	< 4.0
Au/AC-$F_{1.5}I_{1.5}$	< 4.0	5.6
Au/AC-F_2I_2	4.3	17.1
Au/AC-F_0I_1	6.8	9.4

Table S4 EXAFS fitting parameters at the Au L_3-edge for various samples（S_0^2=0.81）

Sample	Shell	N^a	R(Å)^b	$\sigma^2\times10^3$(Å^2)^c	ΔE_0 (eV)^d	R factor
Au foil	Au-Au	12*	2.86±0.01	8.4±0.5	4.1±0.8	0.010
AuCl	Au-Cl	3.0±0.3	2.28±0.01	3.8±0.6	10.2±1.2	0.012
$AuCl_3$	Au-Cl	4.5±0.2	2.29±0.01	2.4±0.3	10.4±0.1	0.005
Au/AC	Au-Cl	0.5±0.1	2.26±0.01	1.0±0.4	6.9±3.0	0.006
	Au-Au	8.1±0.8	2.86±0.01	7.1±0.6	4.4±0.9	
Au/AC-F_1I_1	Au-Cl	1.4±0.1	2.28±0.01	1.7±0.8	10.6±1.4	0.010
	Au-Au	5.6±0.8	2.86±0.01	7.5±0.9	4.1±1.2	

$^a N$: coordination numbers; $^b R$: bond distance; $^c\sigma^2$: Debye-Waller factors; ^{d} ΔE_0: the inner potential correction. R factor: goodness of fit.